EasyChair Preprint

№ 9459

Numerical Simulation of Three-Dimensional Incompressible Fluid Flow in Curved Pipes: FSI Vs CFD

Manh Hung Nguyen, Trung Tien Trinh, Duc Quyen Vu, Xuan Tung Ta, Trung Dinh Nguyen and Sang Truong Ha

December 12, 2022

Numerical simulation of three-dimensional incompressible fluid flow in curved pipes: FSI vs CFD

Nguyen Manh Hung, Trinh Trung Tien, Vu Duc Quyen, Ta Xuan Tung, Nguyen Trung Dinh, Sang Truong Ha*

Department of Mechanical Engineering, Le Quy Don Technical University, 236 Hoang Quoc Viet, Hanoi, Viet Nam.

*Email: sanght.st@lqdtu.edu.vn

Abstract. The present paper aims to show the numerical results of an incompressible fluid flow in curved pipes for three-dimensional space using a fluid-structure interaction (FSI) model. A tetrahedral element is employed to discretize the Navier-Stokes equation for a fluid part and the elastic model for the solid domain. Strong coupling is used for FSI iteration to satisfy the balance conditions at the fluid-solid interface. The current approach is firstly validated by comparison of numerical solution with experimental data for a 90-degree curved pipe in the rigid wall using the CFD model. In addition, the pressure wave propagation in a straight tube is used for FSI validation. Then the algorithm is adopted for calculating the FSI method for the 90-degree curved pipe. The comparison of the FSI and CFD model is shown in detail in this curved pipe. The present work can be used for bio-mechanical prediction, such as the blood flow in coronary artery vessels.

Keywords: CFD, Curved pipes, incompressible fluid flow, fluid-structure interaction, Navier-Stokes equation.

1. Introduction

The study of pulsatile fluid flows in the laminar regime is particularly interesting in many engineering applications, especially for blood flow in physiological circulation. These flows are characterized by a function of velocity or pressure that varies with time. Among them, the oscillating flow in curved pipes plays an important role and is investigated by many researchers, including experiments and numerical methods [1,2]. Detailed analysis of unstable fluid flow in a curved pipeline is important for several reasons. First, fluid flow in a curved tube is considered a fundamental fluid mechanics problem. Many investigators have studied the analytically fully developed flow; however, it is not straightforward for curved pipes. Therefore, the numerical problem approach seems to be an appropriate way to gain insight into the flow phenomena occurring in the region of curved pipes. Second, the unsteady flow in the curved pipes is also closely related to the flow phenomenon occurring in the coronary/arterial vessels of the vascular problem, which is a very challenging problem at present.

In oscillating flows, the interaction between viscous and inertial effects originates from the deviation of the velocity profile from the parabolic shape of a steady flow. When studying the laminar flow through ducts, even a small curvature has a non-negligible effect on the flow. These effects originate from centrifugal force creating a pressure gradient and secondary flows. The secondary flow in a curved pipe depends on the Womersley parameter, Reynolds number, and Dean number [3]. In the field of cardiology, pulsating flow is of particular interest to blood circulation and vascular aging. There has been much research on flow in curved pipes in previous work; however, most employ rigid models using the CFD approach. Moreover, the effect of elastic walls is mentioned very little. Therefore, this study aims to focus on the unsteady fluid flow in curved pipes in three-dimension by using the FSI model and comparing the results with the CFD approach by numerical method.

2. Numerical method

2.1. Equations for incompressible blood flow

The fluid domain is denoted by Ω^f with the boundary Γ^f. The incompressible Navier-Stokes equations can be written in Ω^f by arbitrary Lagrangian-Eulerian formas follows [4]:

$$\rho\left(\frac{\partial u}{\partial t}+(u-u^*)\frac{\partial u}{\partial x}+(v-v^*)\frac{\partial u}{\partial y}+(w-w^*)\frac{\partial u}{\partial z}\right)=-\frac{\partial p}{\partial x}+\rho g_x+\mu\left(\frac{\partial^2 u}{\partial x^2}+\frac{\partial^2 u}{\partial y^2}+\frac{\partial^2 u}{\partial z^2}\right) \tag{1a}$$

$$\rho\left(\frac{\partial v}{\partial t}+(u-u^*)\frac{\partial v}{\partial x}+(v-v^*)\frac{\partial v}{\partial y}+(w-w^*)\frac{\partial v}{\partial z}\right)=-\frac{\partial p}{\partial y}+\rho g_y+\mu\left(\frac{\partial^2 v}{\partial x^2}+\frac{\partial^2 v}{\partial y^2}+\frac{\partial^2 v}{\partial z^2}\right) \tag{1b}$$

$$\rho\left(\frac{\partial w}{\partial t}+(u-u^*)\frac{\partial w}{\partial x}+(v-v^*)\frac{\partial w}{\partial y}+(w-w^*)\frac{\partial w}{\partial z}\right)=-\frac{\partial p}{\partial z}+\rho g_z+\mu\left(\frac{\partial^2 w}{\partial x^2}+\frac{\partial^2 w}{\partial y^2}+\frac{\partial^2 w}{\partial z^2}\right) \tag{1c}$$

And the continuity equation in Ω^f given by:

$$\frac{\partial u}{\partial x}+\frac{\partial v}{\partial y}+\frac{\partial w}{\partial z}=0 \tag{2}$$

where ρ is the fluid density, u, v, w represents the velocity in x, y, z direction, g_i represents the body force in i-direction, and μ denotes the dynamic viscosity of the fluid. u^*, v^*, and w^* represent the components of mesh velocity, and p is fluid pressure. For the CFD method, the solid wall is assumed to be a rigid body, and the mesh velocity (u^*, v^*, w^*) is set to zero.

Equations (1) and (2) are the governing equations for fluid dynamics. Solving this equation to obtain the velocity and pressure field by the FEM method is described in ref. [4].

2.2. Equation for elastic structure of wall

The structure domain is denoted by Ω^s with the boundary Γ^s. The deformation of the wall in the Lagrangian form is written in three-dimensional Cartesian coordinate system by:

$$\rho^s\frac{\partial^2 d_x}{\partial t^2}=\frac{\partial \boldsymbol{\sigma}_{xx}}{\partial x}+\frac{\partial \boldsymbol{\sigma}_{xy}}{\partial y}+\frac{\partial \boldsymbol{\sigma}_{xz}}{\partial z}+\rho^s g_x \tag{3a}$$

$$\rho^s\frac{\partial^2 d_y}{\partial t^2}=\frac{\partial \boldsymbol{\sigma}_{yx}}{\partial x}+\frac{\partial \boldsymbol{\sigma}_{yy}}{\partial y}+\frac{\partial \boldsymbol{\sigma}_{yz}}{\partial z}+\rho^s g_y \tag{3b}$$

$$\rho^s\frac{\partial^2 d_z}{\partial t^2}=\frac{\partial \boldsymbol{\sigma}_{zx}}{\partial x}+\frac{\partial \boldsymbol{\sigma}_{zy}}{\partial y}+\frac{\partial \boldsymbol{\sigma}_{zz}}{\partial z}+\rho^s g_z \tag{3c}$$

where ρ^s is density of solid, d_x, d_y, d_z represents the displacement in x, y, z direction of solid, and $\boldsymbol{\sigma}_{ij}$ denote the components of stress tensor:

$$\sigma=\begin{pmatrix}\sigma_{xx} & \sigma_{xy} & \sigma_{xz}\\ \sigma_{yx} & \sigma_{yy} & \sigma_{yz}\\ \sigma_{zx} & \sigma_{zy} & \sigma_{zz}\end{pmatrix}=\begin{pmatrix}\sigma^x\\ \sigma^y\\ \sigma^z\end{pmatrix} \tag{4a}$$

$$\sigma_{xy}=\sigma_{yx};\ \ \sigma_{xz}=\sigma_{zx};\ \sigma_{yz}=\sigma_{zy} \tag{4b}$$

The relation of stress and strain can be written by compact form as follows:

$$\begin{bmatrix} \sigma_{xx} \\ \sigma_{yy} \\ \sigma_{zz} \\ \sigma_{xy} \\ \sigma_{yz} \\ \sigma_{zx} \end{bmatrix} = [D] \begin{bmatrix} \varepsilon_{xx} \\ \varepsilon_{yy} \\ \varepsilon_{z\,z} \\ \varepsilon_{xy} + \varepsilon_{yx} \\ \varepsilon_{yz} + \varepsilon_{zy} \\ \varepsilon_{zx} + \varepsilon_{xz} \end{bmatrix} \tag{5}$$

where ε_{ij} is components of strain tensor:

$$\boldsymbol{\varepsilon} = \frac{1}{2}\left\{(\nabla \mathbf{d})^{\mathrm{T}} + (\nabla \mathbf{d}) + (\nabla \mathbf{d})^{\mathrm{T}} (\nabla \mathbf{d})\right\} \tag{6}$$

and:

$$\nabla \mathbf{d} = \begin{pmatrix} \frac{\partial d_x}{\partial x} & \frac{\partial d_x}{\partial y} & \frac{\partial d_x}{\partial z} \\ \frac{\partial d_y}{\partial x} & \frac{\partial d_y}{\partial y} & \frac{\partial d_y}{\partial z} \\ \frac{\partial d_z}{\partial x} & \frac{\partial d_z}{\partial y} & \frac{\partial d_z}{\partial z} \end{pmatrix} \tag{7}$$

The constitutive equations of the solid domain in large deformation are explained in Ref. [5].

2.3. CFD method based on FEM formulation on unstructured grid

In this work, the pressure/velocity variable is linearly/quadratically interpolated in a finite element. Fig. 1 shows a *P2P1* finite element for a tetrahedral element [6], where the pressure variable is allocated on the vertices and the velocity variables are on both vertices and mid-nodes.

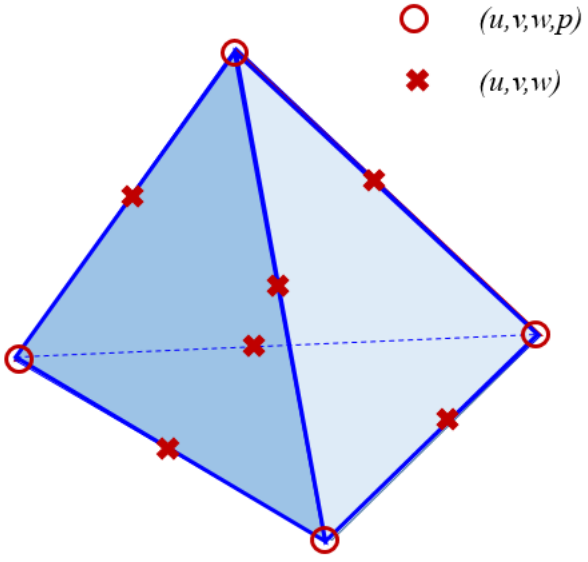

Fig. 1. Degrees of freedom assigned for the *P2P1* finite element [6]

The governing equations (1) and (2) are solved by the fractional method, using the straightforward approach for the non-linear convection term. The body force is neglected in this work. The procedure of the fractional three-step scheme can be written as:

$$\frac{\bar{u}-u^n}{\Delta t}+\left(u^n\frac{\partial\bar{u}}{\partial x}+v^n\frac{\partial\bar{u}}{\partial y}+w^n\frac{\partial\bar{u}}{\partial z}\right)=\frac{\mu}{\rho}\left(\frac{\partial^2\bar{u}}{\partial x^2}+\frac{\partial^2\bar{u}}{\partial y^2}+\frac{\partial^2\bar{u}}{\partial z^2}\right) \tag{8a}$$

$$\frac{\bar{v}-v^n}{\Delta t}+\left(u^n\frac{\partial\bar{v}}{\partial x}+v^n\frac{\partial\bar{v}}{\partial y}+w^n\frac{\partial\bar{v}}{\partial z}\right)=\frac{\mu}{\rho}\left(\frac{\partial^2\bar{v}}{\partial x^2}+\frac{\partial^2\bar{v}}{\partial y^2}+\frac{\partial^2\bar{v}}{\partial z^2}\right) \tag{8b}$$

$$\frac{\bar{w}-w^n}{\Delta t}+\left(u^n\frac{\partial\bar{w}}{\partial x}+v^n\frac{\partial\bar{w}}{\partial y}+w^n\frac{\partial\bar{w}}{\partial z}\right)=\frac{\mu}{\rho}\left(\frac{\partial^2\bar{w}}{\partial x^2}+\frac{\partial^2\bar{w}}{\partial y^2}+\frac{\partial^2\bar{w}}{\partial z^2}\right) \tag{8c}$$

$$\frac{\partial^2 p^{n+1}}{\partial x^2}+\frac{\partial^2 p^{n+1}}{\partial y^2}+\frac{\partial^2 p^{n+1}}{\partial z^2}=\frac{\rho}{\Delta t}\left(\frac{\partial\bar{u}}{\partial x}+\frac{\partial\bar{v}}{\partial y}+\frac{\partial\bar{w}}{\partial z}\right) \tag{9}$$

$$u^{n+1}=\bar{u}-\frac{\Delta t}{\rho}\frac{\partial p^{n+1}}{\partial x} \tag{10a}$$

$$v^{n+1}=\bar{v}-\frac{\Delta t}{\rho}\frac{\partial p^{n+1}}{\partial y} \tag{10b}$$

$$w^{n+1}=\bar{w}-\frac{\Delta t}{\rho}\frac{\partial p^{n+1}}{\partial z} \tag{10c}$$

where Δt is the time step; the superscript n denotes the time level. In this procedure, the intermediate velocity $\bar{u}$, $\bar{v}$, and $\bar{w}$ are solved by the momentum equation (8). Then, the pressure is obtained by solving the Poisson equation (9), and finally the velocity is corrected by using the calculated pressure (10).

Equations (8), (9), and (10) are called strong formulations, and weak formulations are obtained by multiplying two sides of these equations with test functions and applying the divergence theorem. Finally, linear systems are obtained on each equation of (8), (9), and (10). An iterative solution (e.g., conjugate gradient) is employed to solve these linear systems to get the velocity and pressure field at each time level.

2.4. FSI formulations

The governing equations for solid deformation (3) with constitutive equations (5) and (7) are discretized by the Galerkin method on the 10-node tetrahedral element (Fig.1). The stress-strain relation in equation (6) is non-linear with respect to displacement **d**. The Lagrangian method is used for this geometry non-linearity. The FEM discretization for solid deformation was explained in previous works [6]. This section shows the coupling of incompressible fluid flow and elastic structure at the interface.

Let denote the fluid and solid domains (FS interface) interface by Γ^{fs}, $\Gamma^{fs}=\Gamma^f\cap\Gamma^s$. In the implicit coupling method, the velocity and traction need to satisfy the continuum conditions at the interface. When a no-slip condition is applied, the velocity of the fluid is similar to that of a solid on Γ^{fs}, and the balance condition can be written as follows:

$$u=\frac{\partial d_x}{\partial t};\quad v=\frac{\partial d_y}{\partial t};\quad w=\frac{\partial d_x}{\partial t} \tag{11}$$

Due to the force equilibrium condition, the traction should also be continued along the FS interface:

$$\begin{aligned}\boldsymbol{\sigma}_x^s \cdot \mathbf{n}^f &= -\boldsymbol{\sigma}_x^f \cdot \mathbf{n}^s \\ \boldsymbol{\sigma}_y^s \cdot \mathbf{n}^f &= -\boldsymbol{\sigma}_y^f \cdot \mathbf{n}^s \\ \boldsymbol{\sigma}_z^s \cdot \mathbf{n}^f &= -\boldsymbol{\sigma}_z^f \cdot \mathbf{n}^s\end{aligned} \tag{12}$$

It is noted that the direction of the unit normal vector of solid $\mathbf{n}^s$ is opposite to that of fluid $\mathbf{n}^f$ when the grids of fluid and solid domain along the FS interface are conformed.

The flow chart of the fluid-structure interaction is illustrated in Fig. 2. The fluid solver to calculate velocity and pressure is conducted first in each iteration using the Dirichlet condition in equation (11). The traction of fluid acting on the solid wall is computed using the computed velocity and pressure. This traction is the Neumann boundary condition in equation (12) for a solid solver. A convergence checking is performed for displacement at the interface. The solution is convergence when this displacement is not changed with the previous iteration, and the next time step is carried out. Otherwise, the process is continued and repeated for the next iteration.

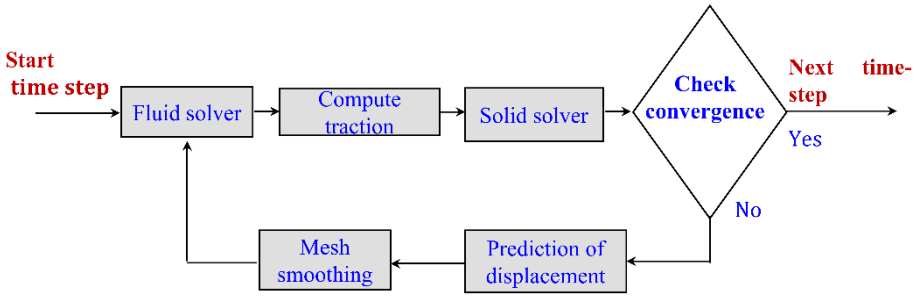

Fig. 2. Flow chart of FSI coupling method

3. Results and discussions

Firstly, the CFD code is validated for the curved pipes by comparing it with experiment data. In addition, a fluid-structure interaction code is confirmed with previous results. Then the FSI code is employed to simulate the case of the curved pipes. Finally, some discussions and the comparison of CFD and FSI modules will be drawn. All the simulations in this work are carried out on a desktop PC, and the code was implemented by Fortran 90 language programming.

3.1. CFD validation for curved pipes

Firstly, a CFD code is validated by comparison of numerical results with experimental data and previous works for the 90-degree curved pipe. The geometry of the benchmark test case, as provided in Refs [1, 2], is shown in Fig. 3. The pipe with a radius of a = 4 *mm* and a curvature radius R = 24 *mm*. A tetrahedral element is used for this three-dimension test case. We only simulate a half domain because of symmetry; the grid is shown in Fig. 4. An independent test is carried out, and the comparison of velocity in the y direction is shown in Fig. 5 for three grid resolutions (course grid, medium grid, and fine grid). The medium grid is employed for the next simulation since it is fine enough for accuracy with a short elapsed time.

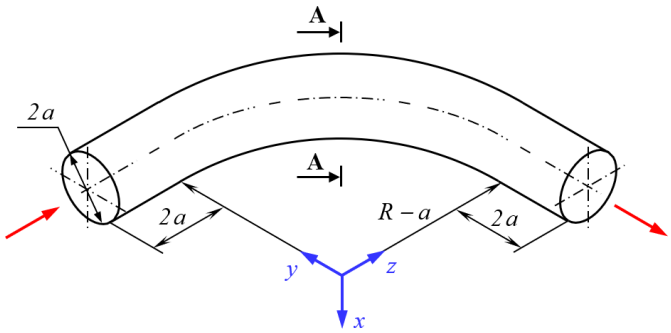

Fig. 3. Geometry of a curved pipe

The code is validated by the two cases: steady and unsteady problems. For the former case, a fully developed profile for the velocity at the inlet is set and the Reynolds number is set by *Re* = 300. A velocity profile at the centerline of section A-A (from inner to outer of the section) is presented in Fig.6 for comparison with previous data. It is clear that the present results are in good agreement with the experimental data as well as the numerical solution of ref [1].

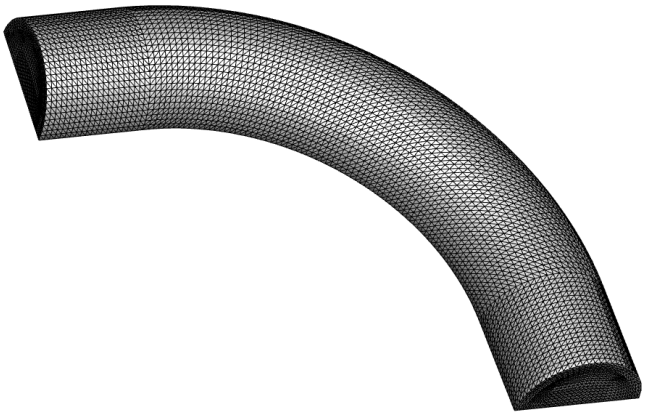

Fig. 4. Tetrahedral element for curved pipe problem

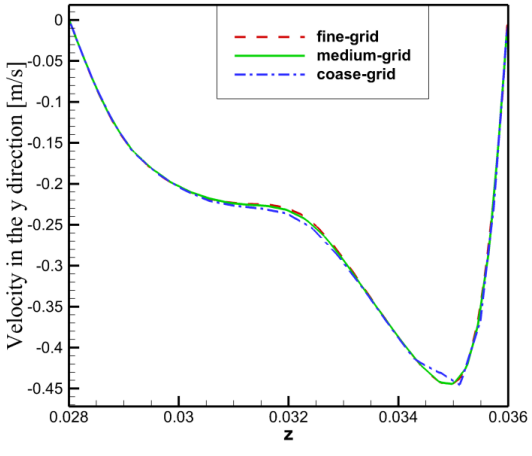

Fig. 5. Velocity in *y* component for test grid

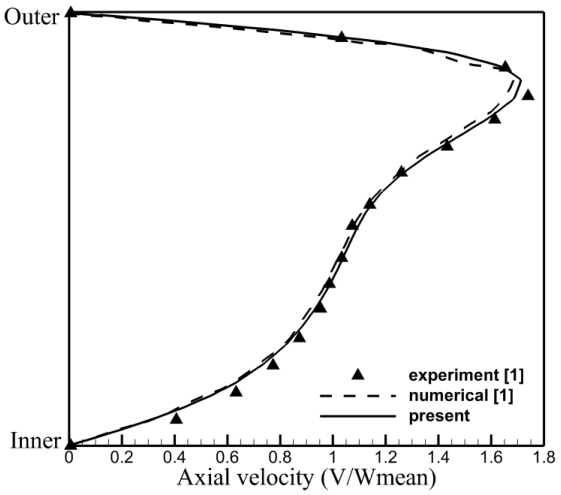

Fig. 6. Validation of steady flow (Re = 300)

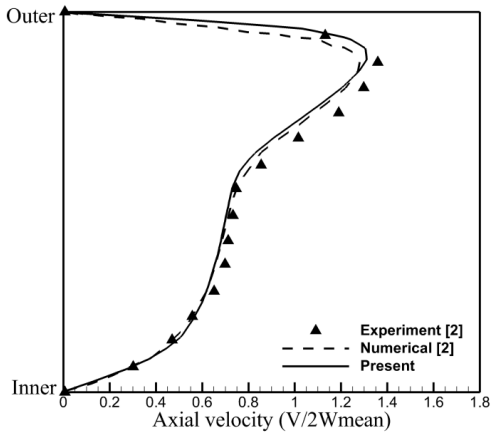

Fig. 7. Validation of unsteady flow ($T/4$)

For the unsteady test case, the boundary condition of ref [2] is adopted, and the comparison of present solutions with those of ref [2] is shown in Fig. 7. Again, the results agreed well with previous works.

3.2. FSI validation

After validating the code for a curved pipe by the CFD method (using a rigid model for the wall), it needs to validate the code for the FSI method. A common benchmark case for FSI validation is the pressure wave propagation in a straight flexible pipe problem. The schematic is shown in Fig. 8. The length and diameter are set by $L = 5.0$ cm and $D = 1.0$ cm, respectively. The thickness of the solid wall is set by $t = 0.1$ cm. The density and viscosity of fluid are $\rho^f = 1.0\ g/cm^3$ and $\mu = 3{\cdot}10^{-3}\ Pa$. The Young's modulus and Poisson ratio for solid walls are set by $\rho^s = 1.2\ g/cm^3$ and $\nu = 0.3$. The detailed simulation setting is provided in ref. [7].

Fig. 9 shows the pressure field and deformation of the solid wall for the two instants time: $t = 0.5\ ms$ and $t = 10\ ms$, which, a factor of 10 for clarity, enhances the wall deformation. The pressure at the centerline at different time instants is plotted in Fig. 10 . It is noted that wave propagation only appears for the elastic wall. For the rigid wall model, the pressure is not changed in time. The displacement and pressure at the inner of the pipe wall are shown in Fig. 11. The present results agree well with previous research in the literature.

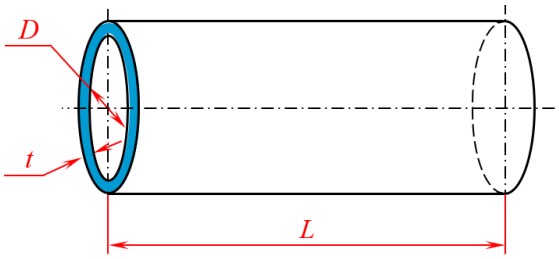

Fig. 8. Geometry of straight pipe problem

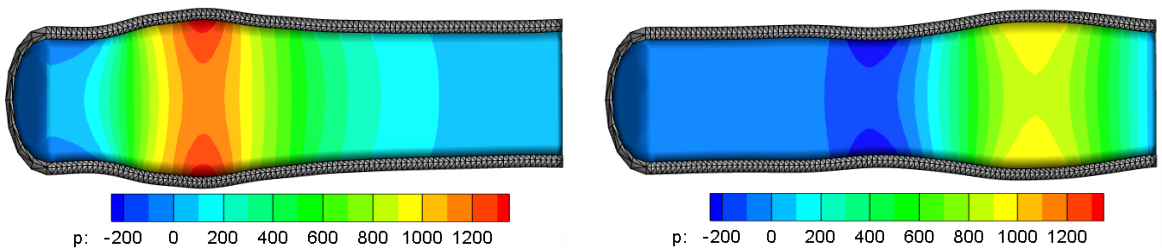

Fig. 9. Pressure field and wall deformation

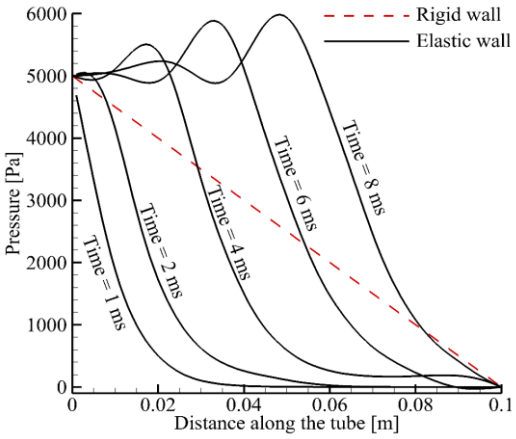

Fig. 10 Pressure at centerline (FSI vs. CFD)

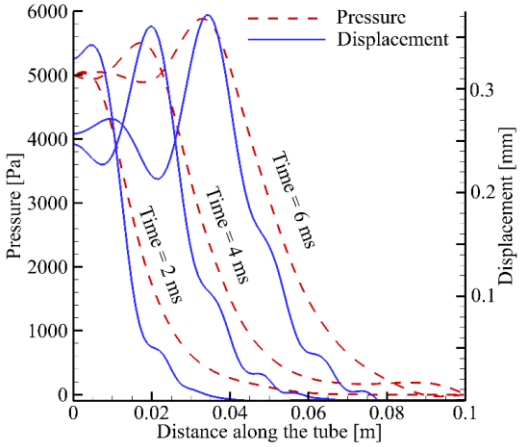

Fig. 11 Pressure and displacement at inner pipe

3.3. FSI effect in 90^0 pipe

Lastly, the FSI model is employed to simulate the curved pipe test. The 90^0 pipe presented in section 3.1 is used for this simulation. Two boundary conditions are employed: Fixed pressure or velocity at the inlet. The outlet is set by zero pressure. For the former case, the comparison of the pressure field is shown in Fig. 12 and Fig. 13 for different instants time. It is shown that the pressure wave propagates along the pipe with a limited velocity. In contrast, the CFD method established nearly the constant pressure gradient for the first time. For the velocity at the inlet case (Re = 600), the comparison of pressure at the centerline is shown in Fig. 14. Fig 15 shows the secondary flow on the section A-A with velocity vector and contour field. Because of wall deformation effect, the elastic wall case by FSI formula shows a little bigger in magnitude velocity near the wall.

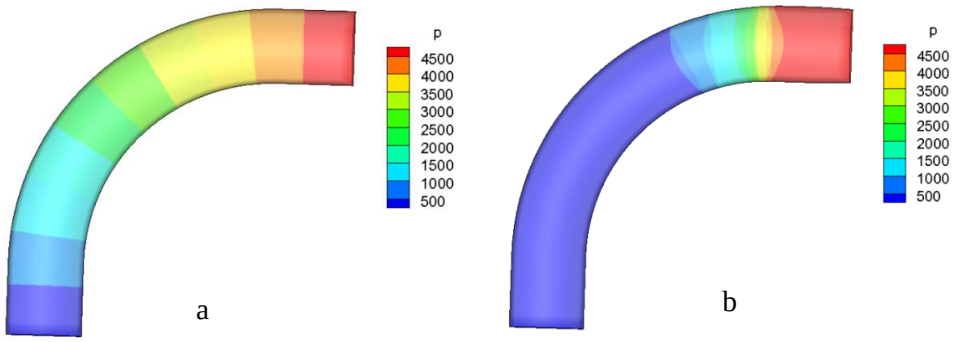

Fig. 12. Pressure contour at time =1.0 *ms* {a) Rigid wall; b) elastic wall}

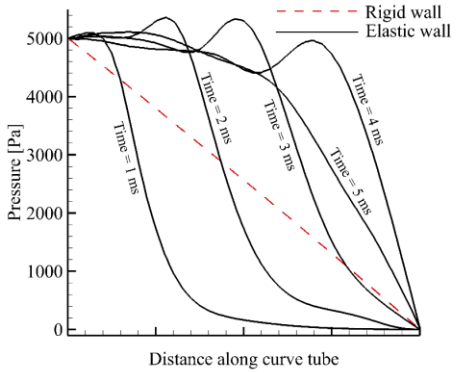

Fig. 13. Pressure at centerline (rigid wall and elastic wall). Pressure boundary condition at inlet.

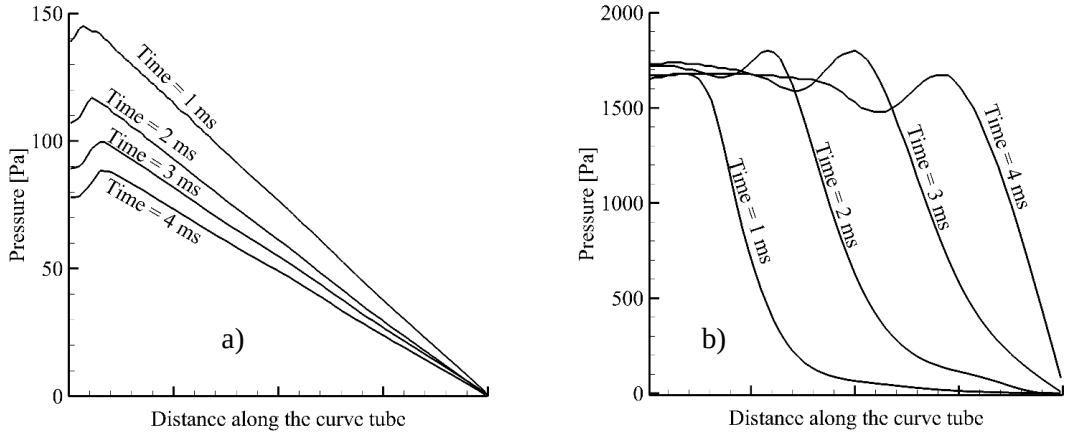

Fig. 14. Pressure at centerline (Velocity boundary condition at inlet, Re = 600): a) Rigid wall, b) Elastic wall

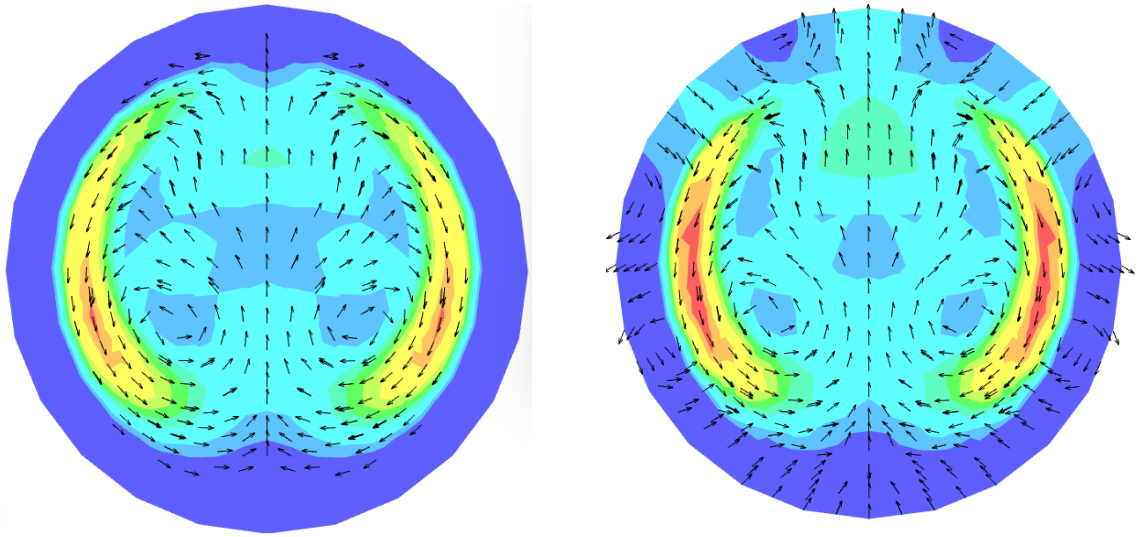

Fig. 15. Secondary flow on section A-A (Re = 600): a) Rigid wall, b) Elastic wall

4. Conclusion

The present work used FSI and CFD formulas to investigate the incompressible flow in curved pipes. The 10-node tetrahedral element was employed for both the fluid and structure grids. The incompressible flow was solved using the fractional step scheme, and the Lagrangian method was used to handle the nonlinear behavior of the stress-strain relation. For the CFD method, the wall was fixed, and a non-slip condition was applied to this boundary. On the other hand, the FSI method employed a moving wall for the fluid solver, and the grid was updated every time-step to avoid lousy quality elements. CFD and FSI methods were validated by comparing the results with experimental data or previous numerical solutions. From the numerical results, the CFD method could not provide an exact solution for the pressure propagation wave since the pressure was nearly developed in the full domain at the first time step. Similar results for the 90-degree curved pipe, the effect of the deformed wall was depicted on both boundary conditions. This study can be employed for simulating the blood flow in the coronary/artery in the human body because the effect of the curved pipe and an elastic wall are significant in these problems.

References

[1] F. N. Van de Vosse, A. A. Van Steenhoven, A. Segal, J. D. Janssen. A finite element analysis of the steady laminar entrance flow in a 90^0 curved tube. *International journal for numerical methods in fluids*, **9.3,** (1989), pp. 275-287.

[2] C. C. M. Rindt, A. A. Van Steenhoven, J. D. Janssen and G. Vossers. Unsteady entrance flow in a 90^0 curved tube. *Journal of Fluid Mechanics*, **226**, (1991), pp. 445-474.

[3] D. P. De Andrade, J. M. C. Pereira and J. C. F. Pereira. Prediction of pulsatile 3D flow in elastic tubes using STAR CCM+ code. In *Proceedings of the 11th World Comgress on Computational Mechanics*, Barcelona, (2014), pp. 20-25.

[4]. T. S. Ha, T.D. Nguyen, V. C. Vu, M. H. Nguyen, M. D. Nguyen. A Study of Fluid-Structure Interaction of Unsteady Flow in the Blood Vessel Using Finite Element Method. In *Proceedings of ICOMMA 2020*, Hochiminh City, (2020), pp. 1089-1101.

[5] G. A. Holzapfel. Nonlinear solid mechanics: A continuum approach for engineering Science. *Meccanica*, **37**, (4/5), (2002), pp. 489 – 490.

[6] T. S. Ha, V. C. Vu, M. H. Nguyen, and M. D. Nguyen. Numerical simulation for fluid-structure interaction of a blood flow with the aortic valve using the fem monolithic formulation. *Journal of Science and Technique*, **16,** (03), (2021), pp. 49-60.

[7] J. Degroote, R. Haelterman, S. Annerel, P. Bruggeman and J. Vierendeels. Performance of partitioned procedures in fluid–structure interaction. *Computers & Structures*, **88**, (7-8), (2010), pp.446–457